Polarization visualization and selection of biotissue image two-layer scattering medium

O. V. Angelsky
A. G. Ushenko
D. N. Burkovets
Yu. A. Ushenko
Chernivtsi National University
2 Kotsyubinsky Str.
Chernivtsi, 58012
Ukraine
E-mail: ushenko@itf.cv.ukrtel.net

Abstract. We analyze and experimentally test the concept of laser polarization biotissue probing. The methods of increasing the SNR in coherent images of the optically anisotropic architectonics of the morphological biotissue structure are considered. The possibilities of polarization selection and contrasting of such images screened by other biotissues are examined. The influence of the depolarization degree of the scattered background on the SNR is investigated. The possibilities of polarization correction of the probing beam for contrasting biotissue images are analyzed. [DOI: 10.1117/1.1854674]

Keywords: signal-to-noise ratio; scattering; scanning; detection.

Paper 02001 received Jan. 3, 2002; revised manuscript received Feb. 17, 2004; accepted for publication May 28, 2004; published online Feb. 3, 2005.

1 Introduction

Light-based techniques are becoming an increasingly popular method of probing heavily scattering media such as body tissue (for a review see Ref. 1, also see Ref. 2). For surface tissue or thin tissue samples it is possible to use the coherence or polarization properties of the light.[3–9]

At the same time, the level of depolarization of initially polarized light, as well as the mode of changing the polarization from one type to another[10–15] remain the informative parameters characterizing biological tissue (BT) structure. It was determined that the length of the pathway of light, on which its complete depolarization occurs, is a characteristics of BTs of different morphological structures and pathological states.

It was determined that light can propagate in skin with a length of approx. 1.2 mm, retaining its linear polarization. This enables obtaining informational images of macroinhomogeneities[11–13] and simultaneous recording of the birefringence and optical activity[14,16–22] of BT.

A reasonable choice of the laser beam polarization state remains an urgent task. According to the data obtained[13] different BTs or the same BTs in various pathological or functional states present different reactions to probing by light with linear and circular polarization. At the same time, the problems of polarization selection of images of different layers of BT with a simultaneous increase of the relation to ''signal noise'' in the image of optically anisotropic structures, which are screened by the other BT layer, remain inadequately explored. This can be used in novel elaborations in the field of optical coherence tomography (OCT), connected with direct recording of Mueller matrix images of successively located BT layers.

Therefore, it would be important to extend the theoretical and experimental background of studies of optical properties of biotissues using polarized light at least in two ways. First, it might be important to expand our understanding of the transformation of polarized radiation by biotissues using the formalism of the Stokes vector and the Muller matrix. The second urgent task is to analyze the vector structure of random laser fields aimed at subsequent development of methods for the polarization selection of such fields.

1.1 *Objective of the Paper*

This paper studies the possibilities of using polarization methods to improve the SNR in images of optically anisotropic structures (collagen and myosin networks, hematomas, neoplasms, etc.) in the case when the biotissue being probed is screened by another biotissue. We consider two situations: singly and multiply scattering object scenes.

2 Theoretical Modeling

2.1 *Monolayers—Single Scattering*

2.1.1 *General remarks*

On the basis of information about morphological biotissue structure,[23–25] the following model scheme is suggested. Biotissue generally consists of two phases: amorphous and optically anisotropic ones. The optically anisotropic component of the biotissue possesses two levels of organization—crystalline and architectonics ones.

Optically coaxial organic fibrillae forming collagen, elastin, myosin fibers, mineralized (hydroxylapatite crystals) and organic fibers, etc. can be included in the crystallite level. Architectonic nets of such biotissues as skin derma (SD), muscle (MT), and bone tissues (BnT) are morphologically the most typical.

The architectonics of SD is formed by statistically oriented bundles of collagen fibrillae (Fig. 1). The diameter of the fibrilla is between 0.5 and 2 μm. Parallel bundles of fibrillae form a fiber, the diameter of which is 5 to 7 μm (papilary

Address all correspondence to A. G. Ushenko, Chernivtsi National University, 2 Kotsyubinsky Street, Chernivtsi 58012, Ukraine. E-mail: ushenko@itf.cv.ukrtel.net

1083-3668/2005/$22.00 © 2005 SPIE

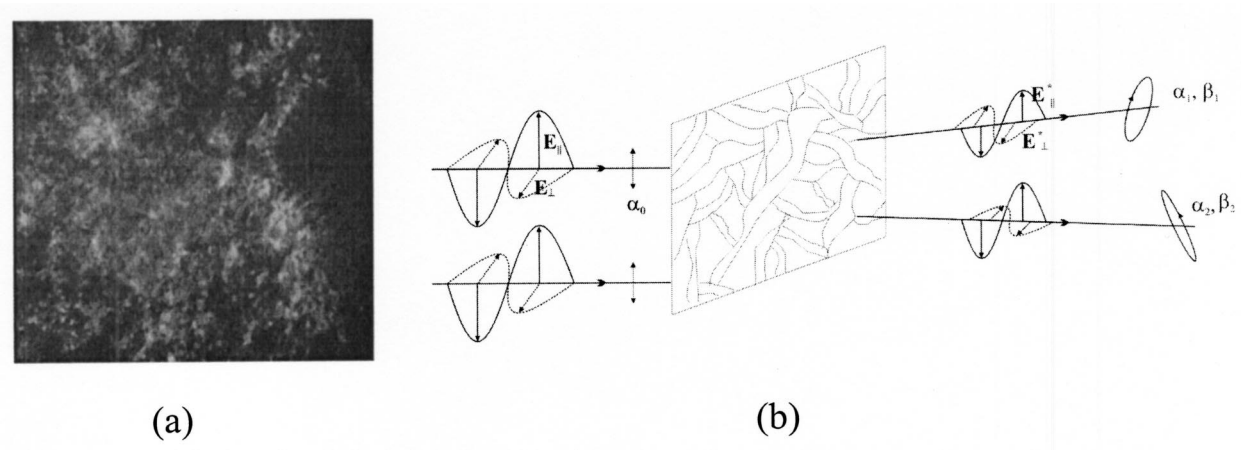

Fig. 1 Model representation of SD architectonics.

layer[23]), and in the net layer, it reaches 30 μm. A collagen bundle, the average diameter of which changes from 100 to 200 μm, is considered to be the highest structural unit of optically active collagen (birefringence value $\Delta n \approx 10^{-3}$).

BnT represents a system, consisting of the trabeculae [Fig. 2(a.1)] layer and osteons [Fig. 2(a.2)]. The optically active matrix consists of hydroxylapatite crystals [$\Delta n \approx 10^{-1}$ (Ref. 24)], the long (optical) axes of which are oriented along the longitudinal axis of collagen fibers [Fig. 2(b)]. They are located between microfibrillae, fibrillae, and collagen fibers, forming a separate continuous mineral phase. Collagen fibers are spatially armored elements in the mineral matrix. The bone trabeculae fiber orientation is ordered and parallel to their plane [Fig. 2(c)]. For BnT osteons, the spatially spiral orientation of the armored collagen fibers is realized.

MT is a structuralized, spatially ordered system of protein bundles, consisting of optically isotropic actin and anisotropic myosin[25] (Fig. 3).

2.1.2 *Optical characteristics*

Optical properties of the primary (crystallite) level of BT organization are characterized by a Mueller operator of the following kind[23]:

$$\mathbf{Q}=\begin{Vmatrix} 1 & 0 & 0 & 0 \\ 0 & [\sin^2(\delta/2)\cos 2\rho+\cos^2(\delta/2)] & [0.5\sin 4\rho \sin^2(\delta/2)] & (-\sin 2\rho \sin\delta) \\ 0 & [0.5\sin 4\rho \sin^2(\delta/2)] & [-\sin^2(\delta/2)\cos 2\rho+\cos^2(\delta/2)] & (\cos 2\rho \sin\delta) \\ 0 & (\sin 2\rho \sin\delta) & (-\cos 2\rho \sin\delta) & [2\cos^2(\delta/2)-1] \end{Vmatrix}. \quad (1)$$

Here ρ is the orientation of optical axis resulting from the direction of the packing of anisotropic fibrillae (collagen myosin, elastin, hydroxyapatite, etc.); and δ is the value of phase shift, performed by their substance between ordinary and nonordinary waves.

2.2 *Two-Layer Scattering Medium*

Recently applications of the Monte Carlo technique in optics of BT have been successfully developed.[26–29] The known algorithms enable us to take into account several BT layers with various optical properties. With its high accuracy and universality, the time factor remains the main drawback of Monte Carlo techniques.

The elaboration of new Mueller matrix OCT (MMOCT) techniques[30–38] requires the creation of efficient, comparatively practical methods of probing the polarization of BT, based on the mathematical formalisms of Stokes vectors and Mueller matrices.

Let a light field, described by Stokes vector $\mathbf{S}^{(0)}$, propagate within a two-layer optically heterogeneous medium (Fig. 4). Due to light-scattering on the heterogeneity of the first layer, the biotissue under study is irradiated by a beam with another Stokes vector $\mathbf{S}^{(1)}=\mathbf{YS}^{(0)}$, where $\mathbf{Y}$ is a matrix of radiation light scattering resulting from the screening biotissue layer.

During the interaction of radiation with the subsurface layer an object field is formed, the polarization characteristic features of which can be described by the vector $\mathbf{S}^{(2)}=\mathbf{XYS}^{(0)}$. Here $\mathbf{X}$ is a matrix of the light scattering of the investigated biotissue.

The radiation detector measures the light field, the Stokes vector of which takes the following form: $\mathbf{S}^{(X)}=\mathbf{YXYS}^{(0)}$ and $\mathbf{S}^{(Y)}=\mathbf{YS}^{(0)}$.

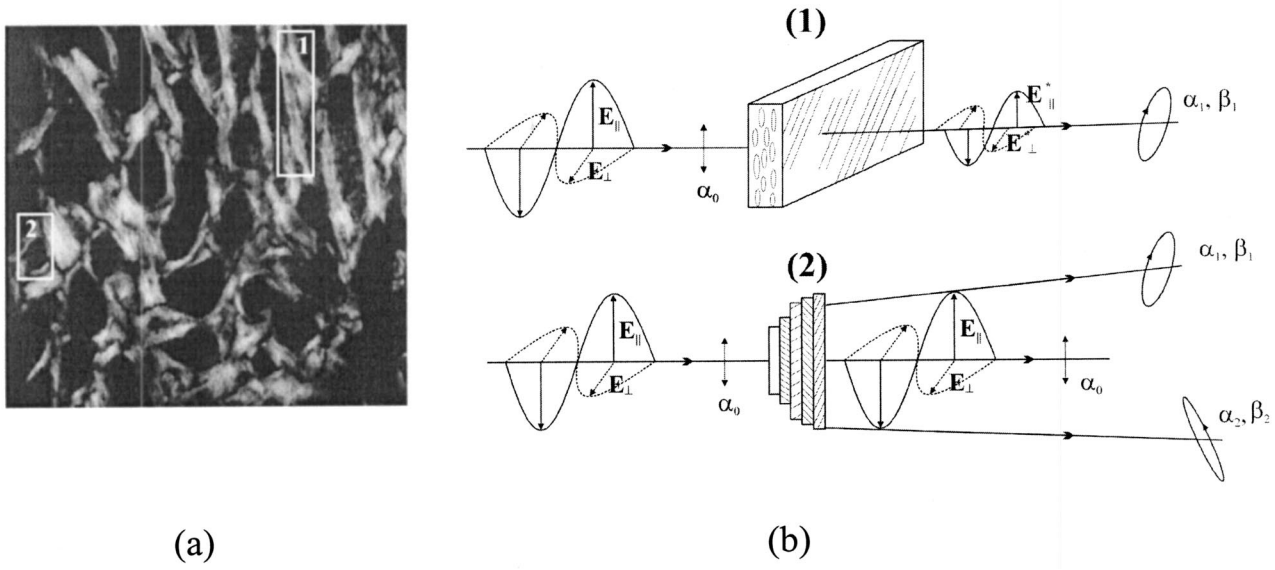

Fig. 2 Model representation of bone tissue structure.

If one takes into account the multiple acts of object reirradiation $[\mathbf{S}^{(3)}]$ and the further outlet of the component of luminous flux into external medium $[\mathbf{S}^{(*)}]$, it is possible to write it as follows: $\mathbf{S}^{(*)}=\mathbf{YXYXYS}^{(0)}$.

Proceeding from the assumption of the independence of the statistical structure of biotissue layers the resulting light field can be presented by the partial vector sum:

$$\mathbf{S}^{(Z)}=\mathbf{S}^{(Y)}+\mathbf{S}^{(X)}+\mathbf{S}^{(*)}, \tag{2}$$

which takes the following matrix form:

$$\mathbf{Z}=\mathbf{Y}+\mathbf{YXY}+\mathbf{YXYXY}+\cdots \tag{3}$$

where $\mathbf{Z}$ is the resulting matrix of light-scattering by a two-layer object scene.

First let us consider the first two constituent parts, i.e., let us assume

$$\mathbf{Y}+\mathbf{YXY}\gg\mathbf{YXYXY}. \tag{4}$$

From an analysis of Eqs. (3) and (4), one can conclude that under determined conditions—i.e., having the information concerning matrices $\mathbf{Z}$ and $\mathbf{Y}$—it is possible to define the matrix $\mathbf{X}$ structure statistically:

$$\mathbf{X}=(\mathbf{Z}-\mathbf{Y})\mathbf{Y}^{-1}\mathbf{Y}^{-1}. \tag{5}$$

Here $\mathbf{Y}^{-1}$ is the inverse matrix of $\mathbf{Y}$.

2.2.1 *Investigation of transformation of types and forms of laser field polarization in heterogeneous object scenes*

Let us consider the possibilities of determining polarization structure of laser radiation scattered by biotissue layers.

It is successfully possible to demonstrate the determination of polarization characteristic features of partial scattered fluxes $(\alpha_x\beta_x;\alpha_y,\beta_y)$ from the following equations:[23]

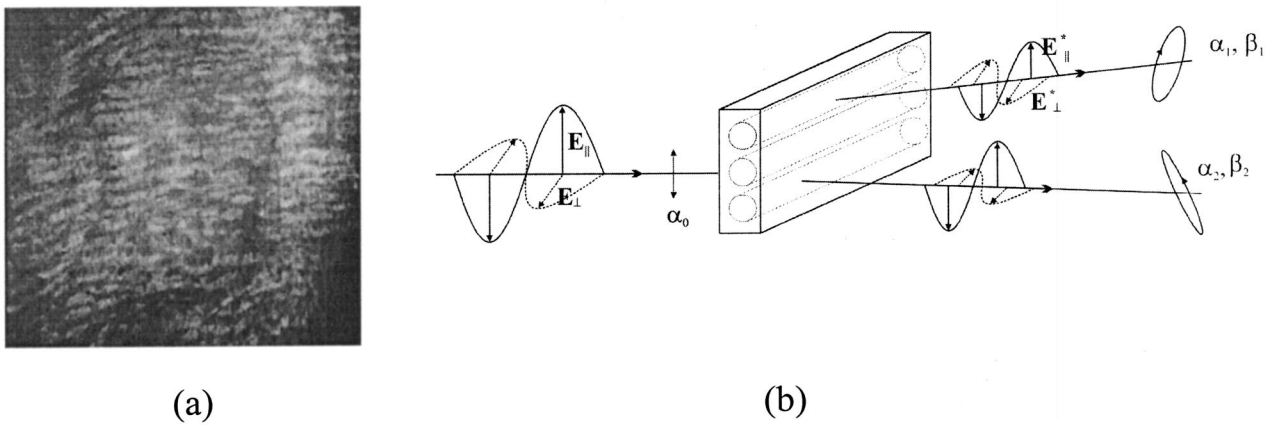

Fig. 3 Model representation of muscle tissue structure.

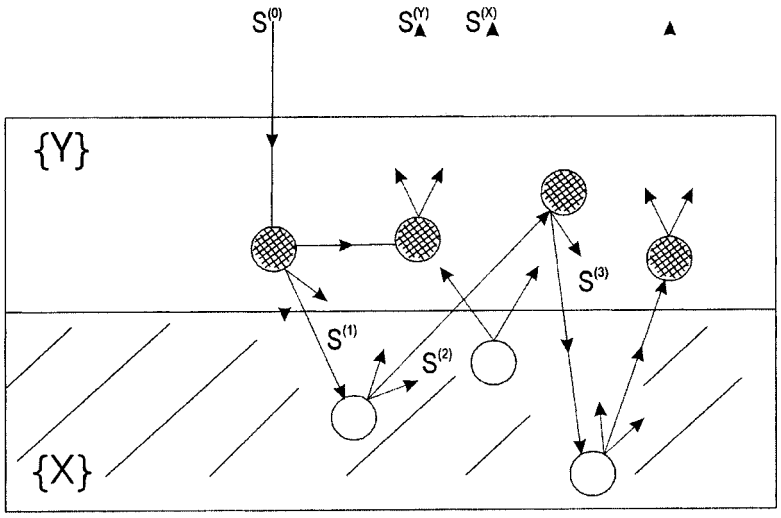

Fig. 4 Model scheme.

$$\alpha_{x,y} = 0.5 \arctan \times \left(\frac{f_{32} \cos 2\alpha_0 \cos 2\beta_0 + f_{33} \sin 2\alpha_0 \cos 2\beta_0 + f_{34} \sin 2\beta_0}{f_{22} \cos 2\alpha_0 \cos 2\beta_0 + f_{23} \sin 2\alpha_0 \cos 2\beta_0 + f_{24} \sin 2\beta} \right), \quad (6)$$

$$\beta_{x,y} = 0.5 \arcsin(f_{42} \cos 2\alpha_0 \cos 2\beta_0 + f_{43} \sin 2\alpha_0 \cos 2\beta_0 + f_{44} \sin 2\beta_0), \quad (7)$$

where α_0 and β_0 are polarization azimuths and ellipticity of the probing laser beam, and f_{ik} are the elements of the partial light-scattering matrices.

Thus, if we have the information concerning matrices **Z** and **Y**, we can ''construct'' matrix **X**, i.e., one is able to determine polarization structure of a signal (α_x, β_x), reflected by the object being probed.

2.2.2 *Technique of polarization—phase information selection in random fields of coherent radiation*

The idea of the technique of polarization-phase extraction of an object image against a background of impediments is based on determining polarization structure $(\alpha_x, \beta_x; \alpha_y, \beta_y)$ of the resulting light field $\mathbf{S}^{(2)}$ by using the measured matrices **Y** and **Z** with the further polarization compensation of a background signal component $\mathbf{S}^{(Y)}$.

One can essentially decrease the intensity value of the scattered background polarization component while the intensity of object signal remains considerable. The latter is possible by placing a polarization filter before the photodetector. The filter consists of an analyzer and quarter-wave plate. Figure 5 demonstrates the mechanism of increasing the relation of ''signal to noise'' (RSN) being determined as follows:

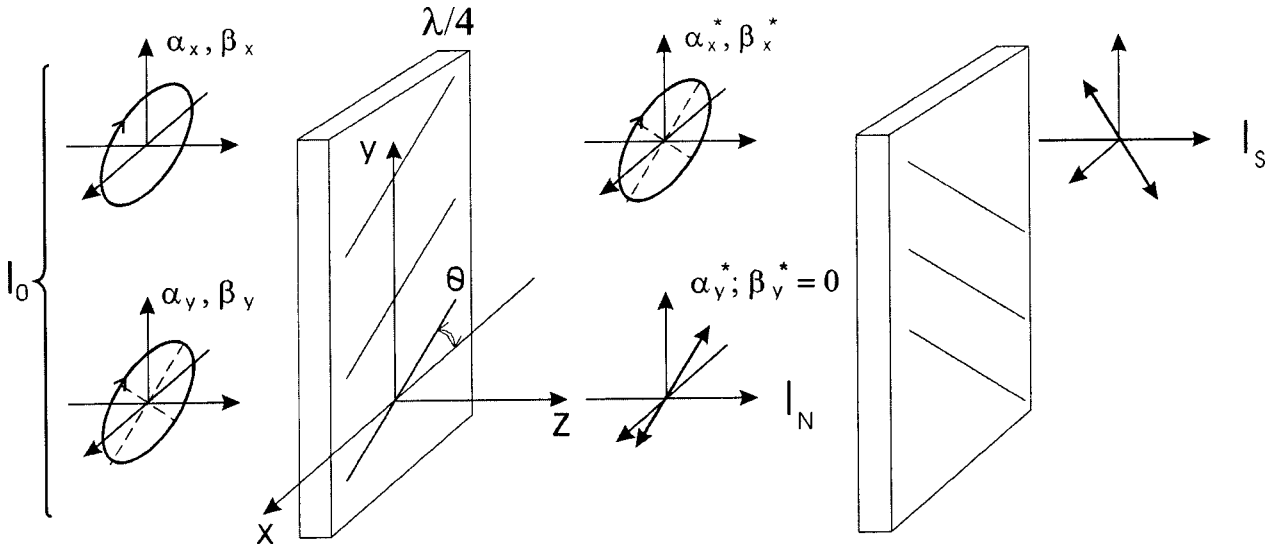

Fig. 5 Scheme of polarization-phase extraction of the informative signal: I_0 is the intensity of the resulting laser beam; and I_S is the output intensity of the informative signal.

$$\eta = 10^3[1-\cos(\alpha_y^*-\alpha_x^*)\cos 2\beta_x^*], \tag{8}$$

where α_y^* is the azimuth of background signal polarization after passing through phase plate $\lambda/4$; and α_x^* and β_x^* are informative signals for the azimuth and ellipticity after passing through the quarter-wave plate. The axis of the latter is oriented in a special way, thus, the ellipticity of background signal polarization $\beta_y^*=0$; the constant 10^3 characterizes the linearity of polarizer-analyzer.

By orienting the greatest speed axis at the angle $\Omega=\alpha_y^*$ one can obtain the following polarization characteristic features of the informative and background signals:

$$\beta_x^* = 0.5\arcsin\{\cos 2\beta_x \sin[2(\theta-\alpha_x)]\}, \tag{9}$$

$$\alpha_x^* = 0.5\arccos \times\left\{\frac{0.5\cos 2\beta_x[\cos(4\theta-2\alpha_x)+\cos 2\alpha_x]\sin 2\beta_x \sin 2\theta}{\cos 2\beta_x^*}\right\}, \tag{10}$$

$$\alpha_y^* = 0.5\arccos\{0.5\cos 2\beta_y[\cos(4\theta-2\alpha_y) - \sin 2\beta_y \sin 2\theta]\}, \tag{11}$$

$$\beta_y^* = 0. \tag{12}$$

Thus, the RSN within the optical field under registration has the value

$$\eta_0 = \frac{I_S}{I_N} = \frac{P_S I_S + \Delta_S I_S}{P_N I_N + \Delta_N I_N}, \tag{13}$$

where I_S and I_N are the intensities of informative and background signals, respectively (Fig. 5); and P_S, Δ_S, P_N, and Δ_N are the polarization and depolarization levels of these components of the scattered radiation field.

By orienting the greatest speed axis of the phase element at the angle $\pi/2+\alpha_x^*$, it is possible to increase the RSN level like this:

$$\eta_s = \frac{P_S I_S \cos^2 \varsigma + 0.5\Delta_S I_S}{kP_N I_N + 0.5\Delta_N I_N}, \tag{14}$$

where $k=10^{-3}$ is the level of radiation intensity of a completely polarized signal component passed through the analyzer; and ζ is the angle between the fluctuation area of electrical intensity vector of completely polarized constituent part of informative signal and analyzer axis direction A (Fig. 5). In addition 50% of the intensity of the completely depolarized constituent parts is passed through the analyzer. Thus, the increase of the RSN ratio resulting from using the polarization compensation technique has the following value:

$$\eta = \frac{\eta_s}{\eta_0} = \frac{P_S \cos^2 \varsigma + 0.5\Delta_S}{kP_N + 0.5\Delta_N}, \tag{15}$$

where

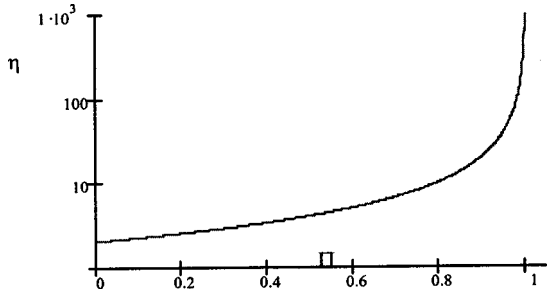

Fig. 6 Level of the SNR as a function of the depolarization degree of the background signal.

$$\cos^2 \varsigma = \frac{\sin^2(\alpha_y^*-\alpha_x^*)+\cos^2(\alpha_y^*-\alpha_x^*)\tan^2\beta_x^*}{1+\tan^2\beta_x^*}. \tag{16}$$

An analysis of Eqs. (15) and (16) shows that maximal level of the RNS is achieved if the following conditions are fulfilled:

$$\varsigma \to \frac{\pi}{2}, \qquad \beta_y^* \to 0. \tag{17}$$

3 Computer Modeling, Analysis, and Discussion

3.1 *Single Scattering*

Figure 7 presents the results of computer modeling the distributions of the coefficient $\eta(\alpha_0,\Theta)$ for an object scene with the following parameters of birefringence: $\Delta n_x=0.1$, $\Delta n_y=0.03$ [Fig. 7(a)], and 0.08 [Fig. 7(b)], and the preferable directions of orientations of biotissues architectonics fibers: $\Delta\rho=\rho_x-\rho_y=20$ deg [see Eq. (1)]. The results of these calculations enable us to make the following conclusions:

1. The efficiency of polarization selection of the informative signal is highly sensitive to the azimuthal geometry of the probe. The coefficient $\eta(\alpha_0,\Theta)$ has a rather complicated topological distribution, and the value of this coefficient ranges from 0 to $\mu=10^3$.
2. The extremal level of $\eta(\alpha_0,\Theta)$ for all the angular arrangements is localized around the azimuthal angle of polarization of the probing beam $\alpha_0=\Delta\rho$.
3. The decrease in the difference of anisotropy levels (Δn_x and Δn_y) in biotissues is accompanied by the formation of additional extrema $[\eta(\alpha_0,\Theta)]/_{\Theta_i=\text{const}}$ for all the values of azimuthal angles α_0.

Let us analyze these results. As follows from boundary conditions [Eq. (17)], the extrema increase in the SNR is achieved when the background signal is linearly polarized. In this case, the intensity of the background signal can be reduced to the level of $\mu^{-1}I_N$. Such a background suppression is achieved when the azimuth α_0 coincides with the anisotropy direction ρ_y of screening biotissue (this direction is mea-

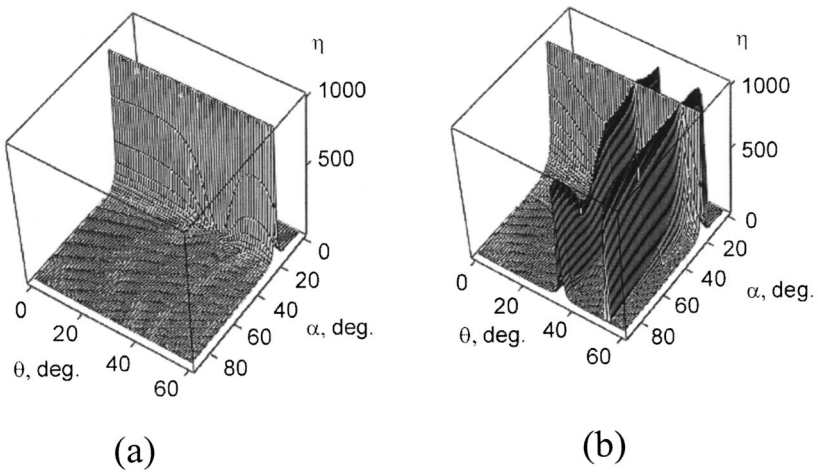

Fig. 7 Dependencies of the improvement factor of the SNR, where θ is scattering angle.

sured from ρ_x), i.e., $\alpha_0=\Delta\rho$. Thus, an extreme line should exist in the distribution $\eta(\alpha_0,\Theta)$ for all the scattering angles Θ.

On the other hand, Eqs. (9) to (12) show that the level of the background and informative signals considerably depends on the relations between the partial matrix elements $\{x_{ik}\}$ and $\{y_{ik}\}$. The values of these elements fluctuate in different ways, depending on Δn_x, Δn_y, and Θ (Ref. 23). Therefore, a linearly polarized background and the relevant extremum lines $\eta(\alpha_0,\Theta)/_{\Theta_i=\text{const}}$ may be observed within a broad range of α_0 [Figs. 7(b)].

Figure 8 displays the dependences characterizing the transformation of the polarization structure of the background (I_N) and informative (I_S) signals in response to variations in the azimuth α_0 of the probing beam. These results were obtained for the following scattering angles: $\Theta=0$ deg [Figs. 8(a) and 8(d)], $\Theta=35$ deg [Figs. 8(b) and 8(e)], and $\Theta=55$ deg [Figs. 8(c) and 8(f)]. The left-hand column corresponds to anisotropy parameters $\Delta n_x=0.1$ and $\Delta n_y=0.03$, while the right-hand column corresponds to anisotropy parameters $\Delta n_x=0$, and $\Delta n_y=0.08$.

The analysis of these data reveals a correlation between zero values of the ellipticity of the background signal $\beta_y^*(\alpha_0=\Delta\rho)$ (curves 3) and the extremal level of the improvement factor of the SNR ratio $\eta(\alpha_0,\Theta)\rightarrow\mu$, which is observed for arbitrary values of polarization parameters of the informative signal $\alpha_x^*-\alpha_y^*=\Delta\alpha$ and β_x^* (curves 1 and 2 in Fig. 8).

For other values of the azimuthal angle α_0 of polarization of the probing beam, two field components of scattered laser radiation are generally elliptically polarized. Therefore, the level of the coefficient $\eta(\alpha_0,\Theta)$ becomes much lower, vanishing around $\beta_x^*\approx\beta_x^*$.

The choice of the optimal scattering angle Θ (with $\alpha_0=\Delta\rho$) and the optimal polarization plane for scattering angles corresponding to the extremal situation, $[\eta(\alpha_0,\Theta)]/_{\Theta_i=\text{const}}$, is important for the photometry of the informative signal I_S. This is due to the fact that, when the extremal level $\eta(\alpha_0,\Theta)=\mu$ is achieved, the polarization structure of the informative signal differs for different values of α_0 and Θ.

Figure 8 displays a series of dependences of I_S calculated for the directions $\alpha_0=20$ deg [Fig. 8(a)], $\Theta=35$ deg [Fig. 8(b)], and $\Theta=55$ deg [Fig. 8(c)] of extrema of the coefficient $\eta(\alpha_0,\Theta)$.

Analysis of these results shows that, when the minimum background level ($\mu^{-1}I_N$) is achieved, the informative signal may vary within a broad dynamic range of three orders of magnitude (from 10^{-3} to 1). An optimal photometric situation is achieved when the boundary conditions for the polarization state of the object signal produced by a biotissue [Eqs. (17)] are satisfied.

3.2 *Multiple Scattering*

Let us reconsider the analysis of Eqs. (15) and (16). The bright dependency of η curves on the polarization condition of the probing beam (α_0,β_0) angle characteristics makes the necessity to solve the tasks of polarization optimization, i.e., selection of optimal characteristic features of the probe beam when T is a maximum obtained value. Let us consider first the situation of linearly polarized scattering fields. Let us study function $\eta(\alpha_0)$ for its extremum:

$$\frac{d\eta}{d\alpha}=\frac{\partial\eta}{\partial\xi}\frac{\partial\xi}{\partial\alpha_0}+\frac{\partial\eta}{\partial\beta_x^*}\frac{\partial\beta_x^*}{\partial\alpha_0}=0. \tag{18}$$

One can conclude from Eq. (18) that for polarizational probing of two-layer scattered medium the polarizationally optimal ones will be Eqs. (17). Equations (17) are possible when the polarization azimuth of the probing laser beam satisfies the following conditions:

$$\alpha_0^*=0.5\arctan\frac{q_1+(q_1^2-4q_2q_3)^{1/2}}{2q_3},$$

$$q_1=-[y_{32}(x_{33}+x_{22})+x_{32}(y_{33}+y_{22})], \tag{19}$$

$$q_2=x_{32}y_{23}+x_{22}y_{22},$$

$$q_3=x_{23}y_{32}+x_{33}y_{33}.$$

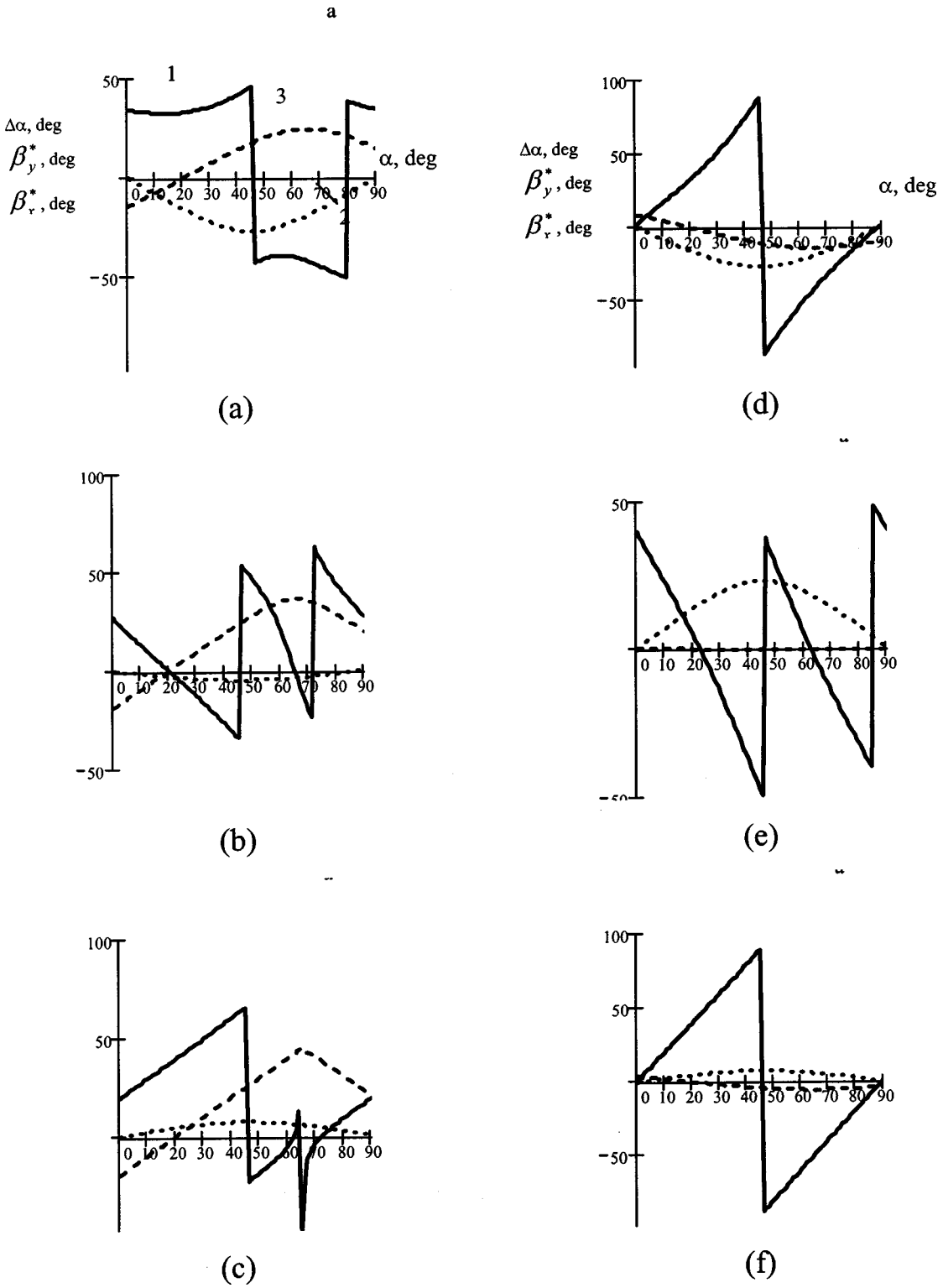

Fig. 8 Polarization structure of the background and informative signals.

Analogous results can be achieved by using polarization ellipticities of the probing beam at the constant value of polarization azimuth ($\alpha_0 = \text{const}$).

The optimal value will be that of polarization ellipticity (Fig. 9), which is defined by the following equation solution:

$$\frac{d\eta}{d\beta} = \frac{\partial \eta}{\partial \xi}\frac{\partial \xi}{\partial \beta_0} + \frac{\partial \eta}{\partial \beta_x^*}\frac{\partial \beta_x^*}{\partial \beta_0} = 0, \tag{20}$$

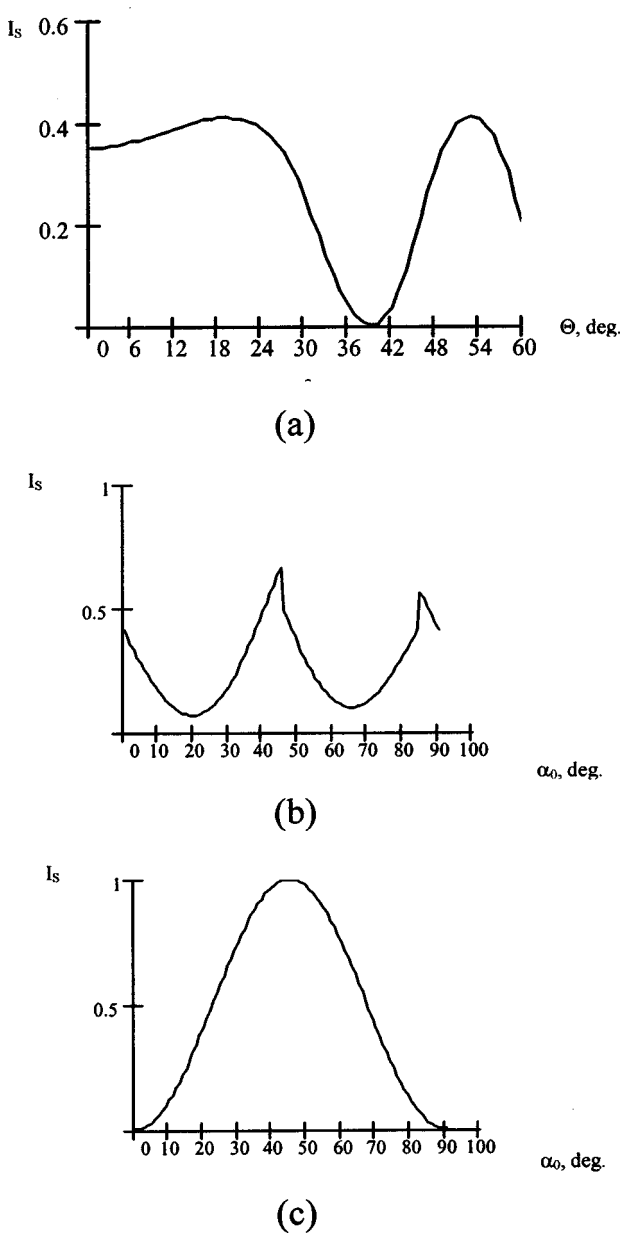

Fig. 9 Transfer function of the informative signal level.

$$\beta_0^* = -0.5 \times \arctan\left[\frac{(x_{32}+x_{22})\cos 2\alpha_0^* + (x_{33}+x_{23})\sin 2\alpha_0^*}{x_{34}+x_{24}}\right]. \quad (21)$$

As we can see from Eq. (15), the depolarization parameter Δ noticeably lowers the improvement factor of the SNR in multiply scattering object scenes. This tendency is shown in Fig. 6, which illustrates the lowering in the improvement factor of the SNR with a decrease in the polarization degree on a logarithmic scale. As we can see from this figure, for $\Pi=(1-\Delta)=0.9$, the coefficient η is reduced by two orders of magnitude, while for $\Pi=0.1$, the factor η decreases further, virtually by another order of magnitude.

On the other hand, the analysis of Eq. (15) shows that the improvement factor of the SNR reaches its extremal level when both conditions of Eq. (17) are satisfied.

3.2.1 *Computer modeling*

Figure 10 presents the results of computer modeling for the ''spatial'' and ''topological'' distributions of the improvement factor of the signal-to-noise ratio η obtained in the cases of single [Figs. 10(a) and 10(b), $\Pi=1.0$] and multiple [Figs. 10(c) and 10(d), $\Pi=0.12$) scattering and in the regime of polarization correction of the probing beam [Figs. 10(e) and 10(f)]. The parameters of the object scene model a sequence of layers of cancellous bony and fibrillar muscular tissues with $\Delta n_x=0.1$, $\Delta n_y=0.03$, and $\Delta\rho=\rho_x-\rho_y=0^0$.

The results of our modeling enable us to make the following conclusions:

1. In the regime of single scattering, the improvement factor of the SNR reaches it extremal level ($\eta\rightarrow 10^3$) for the polarization azimuthal angles α_0 and scattering angles Θ corresponding to a background signal whose vector structure tends to the structure of linearly polarized radiation ($\beta_y\rightarrow$min) [Figs. 11(b) and 11(c)]. Conversely, in the case when the informative and background signals are elliptically polarized ($\beta_y^*\rightarrow$max,$\beta_x^*\rightarrow$max), the coefficient $\eta(\alpha_0,\Theta)\rightarrow$min tends to its minimum vanishing in the limiting case, regardless of the difference of polarization azimuthal angles $\Delta\alpha$ [Fig. 11(a)].
2. In the case of a multiply scattering muscular tissue, the level of η lowers by virtually three orders of magnitude within the entire range of azimuthal angles α_0 and angles Θ. This is due to the fact that the polarization states of the informative and background signals are virtually indistinguishable in this case $\Delta\alpha\rightarrow$min; $\beta_y^*\approx\beta_x^*$ [Figs. 11(d) to 11(f)].
3. Polarization correction of the polarization state of a laser beam probing a multiply scattering object scene increases the improvement factor of the SNR by an order of magnitude for virtually any scattering angle Θ.

4 Automatic Polarimeter Design

The overall layout of the instrument is shown in Fig. 12. The main optical elements of the polarimeter are the He-Ne laser ($\lambda=0.6328$ μm, 10 mW), the polaroid P, two quartz quarter-wave ($\lambda/4$) plates (fourth order), and the polaroid A as the analyzer. By setting the polarization plane of P parallel to the optical axis of the first quarter-wave plate the object under test O (a tissue sample) is illuminated by a linearly polarized light beam, with the analyzer similarly coupled with the second quarter-wave plate.

The He-Ne laser beam is expanded by the afocal system (R) up to the diameter of 3 mm. The pinhole located in the expansion optics removes the scattered light originating from secondary reflections in the resonator and optics contaminations. The role of the half-wave plate $\lambda/2$ is to match the laser beam polarization plane to the polarizer transmittance direction and, at the same time, to control the light level at the CCD matrix to avoid its saturation.

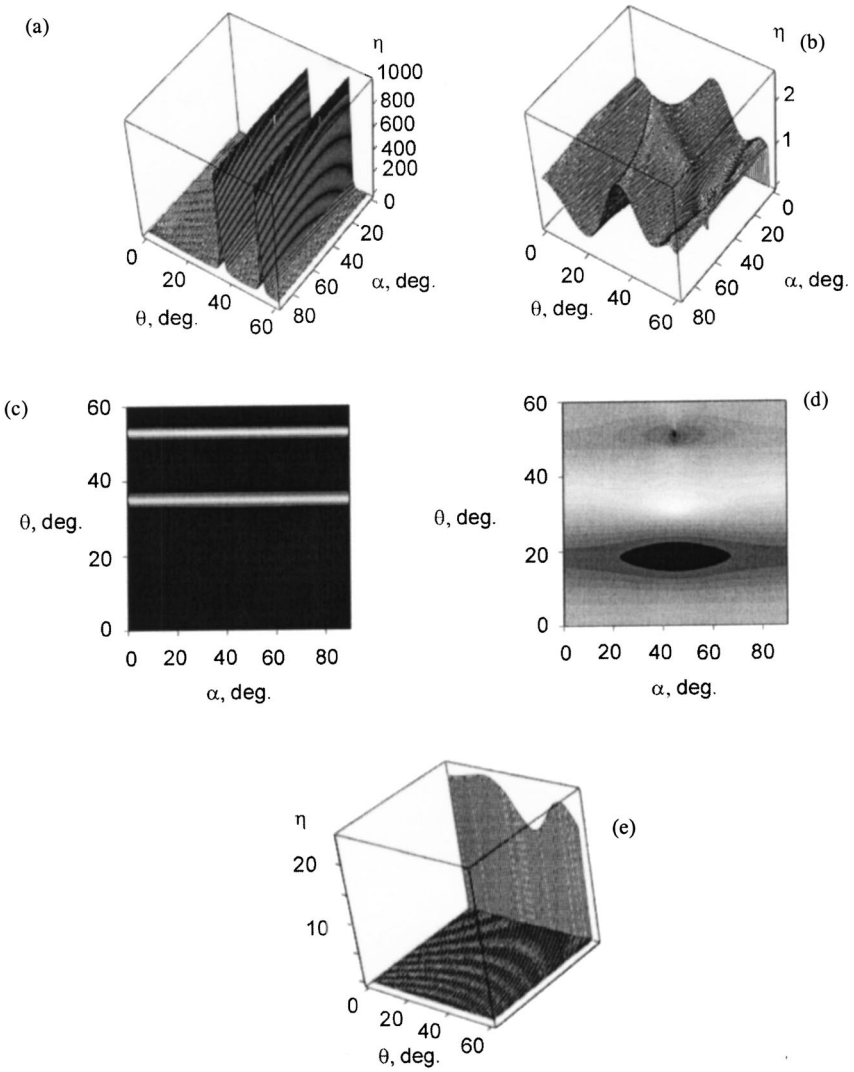

Fig. 10 Spatial-azimuthal and topological dependencies of the SNR improvement factor for singly and multiply scattering biostructures and in the regime of polarization correction of the probing beam.

The tissue sample is placed on the microscope slide. The slide with tissue is fixed in a mount, providing transverse translations in two mutually perpendicular directions in the range of 5 mm to enable us to choose various fragments of the sample.

The sample image is formed on the CCD matrix by the optical system composed of two microscope objectives OL. The overall dimensions of the quarter-wave plate and analyzer driving systems do not enable us to place the imaging optics closer than 200 mm from the sample. The images registered by the CCD matrix and the frame grabber are transferred in a digital form to the computer memory.

The half-wave plate, both quarter-wave plates, the polarizer, and the analyzer are rotated by means of step motors. One motor step corresponds to 22.5 arcmin of the rotation of an optical element.

Before making measurements, the automatic system calibration is performed in the following order:

1. The optical axes of quarter-wave plates are set parallel to transmittance directions of polarizer and analyzer.
2. The transmittance planes of polarizer and analyzer are set parallel.
3. The half-wave plate is rotated to obtain the maximum signal level registered by the CCD matrix (without saturation).
4. Both the analyzer and the second quarter-wave plate are rotated into the crossed position with the polarizer.

5 Experimental Results

Figure 13 presents the results of experimental testing of the method of polarization laser probing of biotissues. Histological slices of biostructures placed in a sequence were employed as objects of our studies. The optical and morphological parameters of these objects correlated with the data of computer modeling.

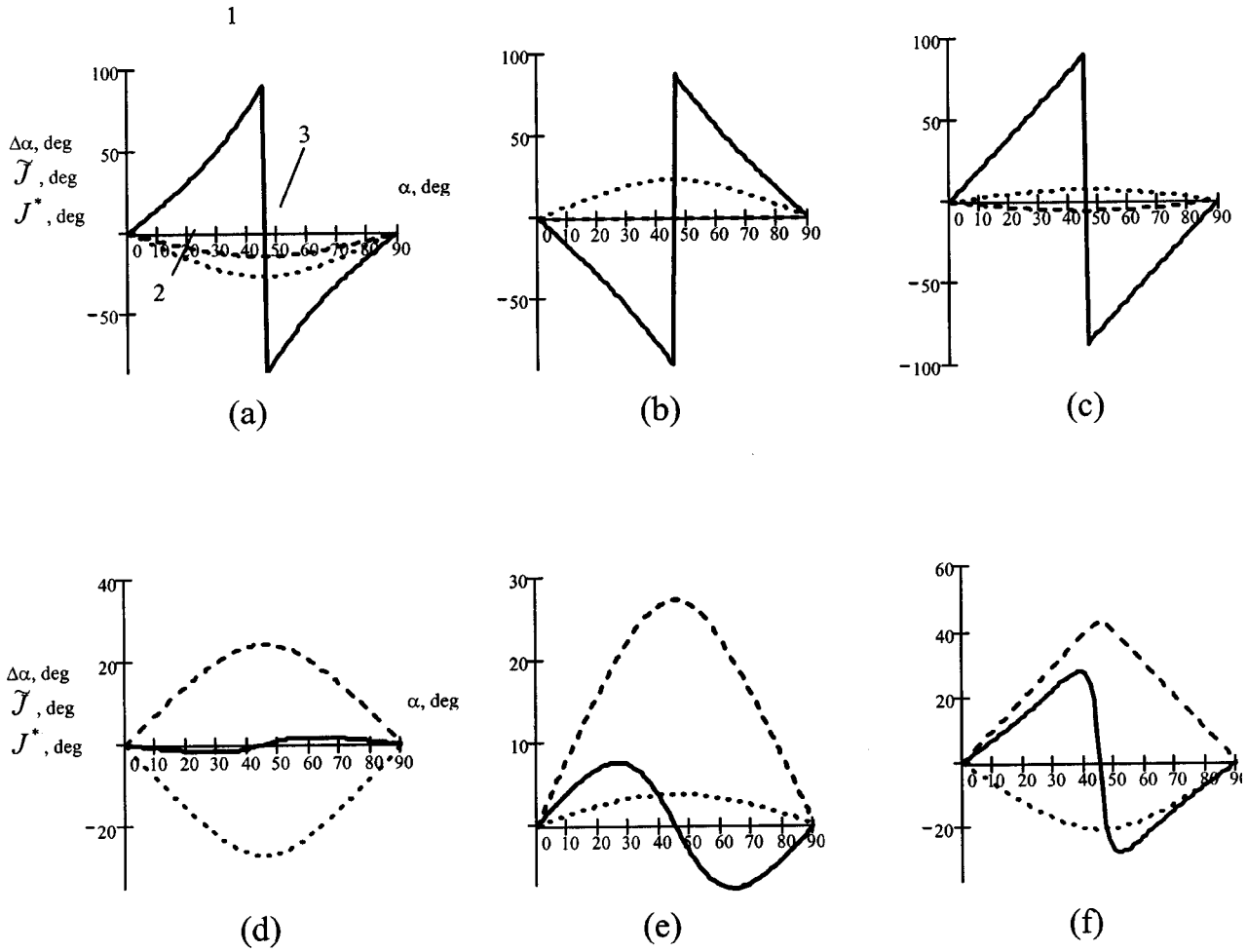

Fig. 11 Polarization structure of the background and informative signals.

As the objects under investigation, the following types of morphological sections of biotissues were used:[39–42]

1. cancellous bone tissue (the absorption coefficient $\mu_a = 2.63\,\mathrm{cm}^{-1}$, the scattering coefficient $\mu_s = 60.02\,\mathrm{cm}^{-1}$, the anisotropy parameter $g = 0.88$, the birefringence index $\Delta n = 0.1$, the geometric thickness $z = 40\ \mu\mathrm{m}$)
2. skin derma ($\mu_a = 2.2\,\mathrm{cm}^{-1}$, $\mu_s = 185\,\mathrm{cm}^{-1}$, $g = 0.82$, $\Delta n = 0.01$, $z = 30\ \mu\mathrm{m}$)
3. fibrillar muscular tissue ($\mu_a = 2\,\mathrm{cm}^{-1}$, $\mu_s = 215\,\mathrm{cm}^{-1}$, $g = 0.96$, $\Delta n = 0.03$, $z = 30\ \mu\mathrm{m}$)

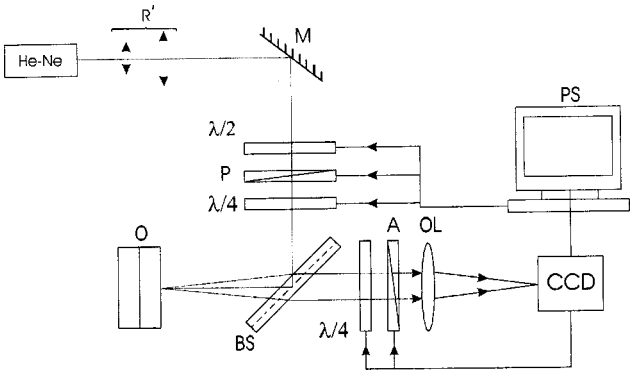

Fig. 12 Optical scheme.

Experiments were performed with the following object scenes, skin derma and cancellous bony tissue for the following parameters $\Delta\rho \approx 20$ deg, $\alpha_0 = 20$ deg [Fig. 13(a)], and $\Theta = 0$ deg [Fig. 13(b)], and fibrillar muscular tissue and derma tissue with $\Delta\rho \approx 20$ deg, $\alpha_0 = 20$ deg [Fig. 13(c)], $\Theta = 0$ deg [Fig. 13(d)], $\Theta = 35$ deg [Fig. 12(e)], and $\Theta = 55$ deg [Fig. 13(f)].

The results of measurements of the coefficient $\eta(\alpha_0, \Theta)$ demonstrate the efficiency of polarization probing of biotissues within a sufficiently broad range of scattering angles, $\Theta < 20$ deg. The discrepancy between the results of computer modeling (solid lines) and experimental data (points) does not exceed 10 to 20% within this range. As the observation angle Θ increases, the coefficient $\eta(\alpha_0, \Theta)$ noticeably decreases, while the discrepancy between theoretical predictions and experimental data may reach 50 to 80%. This effect is apparently due to the increase in the multiplicity of light scattering and the growth in the depolarization of the background signal, which is not included in theoretical modeling. However, even

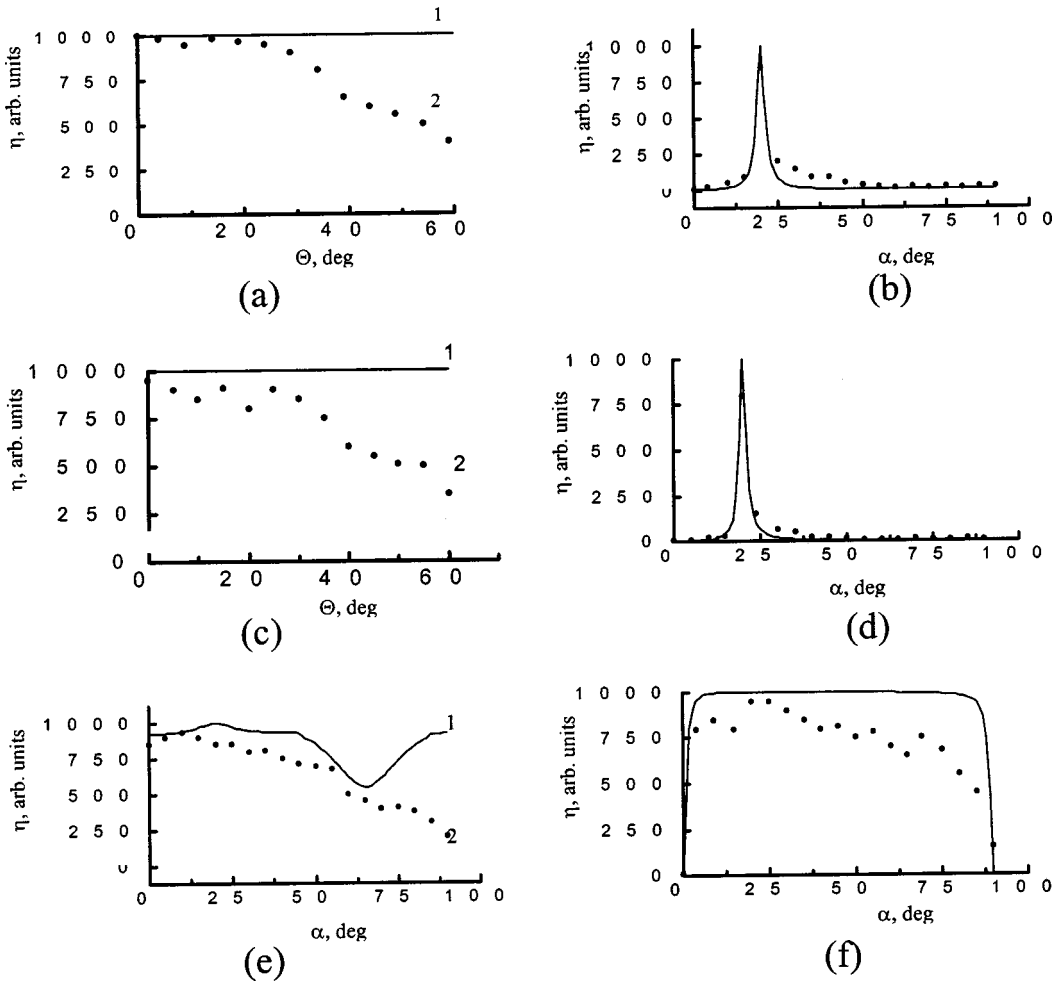

Fig. 13 Experimental dependencies $\eta(\alpha_0,\Theta)$ for single scattering.

in this regime, the improvement factor of the SNR remains sufficiently high: $\eta(\alpha_0,\Theta)\sim 10$ to 100.

The results of experimental testing of the method of laser probing with a fixed polarization state and correction of the azimuth and ellipticity of polarization are presented in Fig. 14. In the figure, curves 1 to 3 were obtained for scattering angles $\Theta=0$, $\Theta=20$, and $\Theta=55$ deg, respectively, illustrating the efficiency of polarization probing of biotissues with a high level of the depolarized background signal. The thickness of shading biotissue (skin derma) was $z=250\ \mu$m. The results of laser probing with polarization correction are presented by curve 4.

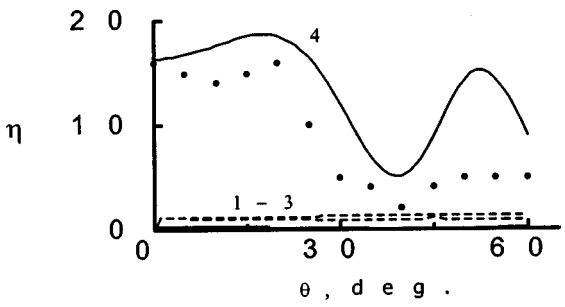

Fig. 14 Experimental dependencies $\eta(\alpha_0,\Theta)$ for multiple scattering.

A comparative analysis of the experimental data reveals the growth in the improvement factor of the SNR by virtually an order of magnitude for any angle Θ.

A comparison with the results of analytical modeling shows a satisfactory agreement between theoretical predictions and experimental data. The level of discrepancies varies from 10 to 30%. Lower SNRs obtained in experiments may be due to some variance of orientations of optically active elements in bony and muscular tissues, which may increase the ellipticity of the object field[19] and a variance of the optical anisotropy of biotissues.

6 Conclusion

In practice, the results obtained may be useful for the development of probing techniques and processing of the obtained BT images in OCT systems, and their novel modifications—MMOCT.

References

1. J. C. Hebden, S. R. Arridge, and D. T. Delpy, ''Optical imaging in medicine: I. Experimental techniques,'' *Phys. Med. Biol.* **42**, 825–840 (1997).
2. Y. T. Pan and D. L. Farkas, ''High-resolution imaging of living human skin with optical coherence tomography,''*Scanning* **21**, 134–135 (1999).
3. J. Welzel, E. Lankenau, R. Birngruber, and R. Engelhardt, ''Optical coherence tomography of the human skin,''*J. Am. Acad. Dermatol.* **37**, 958–963 (1997).
4. S. P. Morgan, M. P. Khong, and M. G. Somekh, ''Effects of polarization state and scatterer concentration on optical imaging through scattering media, '' *Appl. Opt.* **36**, 1560–1565 (1997).
5. S. L. Jacques, J. R. Roman, and K. Lee, ''Imaging superficial tissues with polarized light,'' *Lasers Surg. Med.* **26**, 119–129 (2000).
6. S. G. Demos, H. B. Radousky, and R. R. Alfano, ''Deep subsurface imaging in tissues using spectral and polarization filtering,'' *Opt. Express* **7**, 23–28 (2000).
7. G. Yao and L. Wang, ''Propagation of polarized light in turbid media: simulated animation sequences,'' *Opt. Express* **7**, 198–203 (2000).
8. G. D. Lewis, D. L. Jordan, and P. J. Roberts, ''Backscattering target detection in a turbid medium by polarization discrimination,'' *Appl. Opt.* **38**, 3937–3944 (1999).
9. H. Dehghani, D. T. Delpy, and S. R. Arridge, ''Photon migration in non-scattering tissue and the effects on image reconstruction,'' *Phys. Med. Biol.* **44**, 2897–2906 (1999).
10. H. Horinaka, K. Hashimoto, K. Wada, and Y. Cho, ''Extraction of quasi-straightforward-propagating photons from diffused light transmitting through a scattering medium by polarization modulation,'' *Opt. Lett.* **20**, 1501–1503 (1995).
11. M. R. Ostermeyer, D. V. Stephens, L. Wang, and S. L. Jacques, ''Near field polarization effects on light propagation in random media,'' *OSA TOPS Biomed. Opt. Spectrosc. Diagn.* **3**, 20–25 (1996).
12. A. H. Hielscher, J. R. Mourant, and I. J. Bigio, Imaging superficial tissues with polarized light,'' *OSA TOPS Biomed. Opt. Spectros. Diagn.* **3**, 26–31 (1996).
13. D. Bicout, C. Brosseau, A. S. Martinez, and J. M. Schmitt, ''Depolarization of multiply scattered waves by spherical diffusers: influence of the size parameter,'' *Phys. Rev. E* **49**, 1767–1770 (1994).
14. J. R. de Boer, T. E. Milner, M. J. C. van Gemert, and J. S. Nelson, ''Determination of the depth-resolved Stokes parameters of light backscattered from turbid media by use of polarization-sensitive optical coherence tomography,'' *Opt. Lett.* **22**, 934–936 (1997).
15. H. Hielscher, A. A. Elick, J. R. Mourant, and I. J. Bigio, ''Biomedical diagnostic with diffusely backscattered linearly and circularly polarized light,'' in *Biomedical Sensing, Imaging, and Tracking Technologies II*, R. A. Lieberman, T. Vo-Dinh, and G. G. Vurek, Eds., *Proc. SPIE* **2976**, 298–305 (1997).
16. N. Kollias, in K.-P. Wilhelm, P. Elsner, E. Berardesca, and H. I. Maibach, ''Polarized light photography of human skin, in Bioengineering of the Skin: Skin Surface Imaging and Analysis,'' Eds., pp. 95–106, CRC Press, Boca Raton, FL (1997).
17. A. F. Fercher, ''Optical coherence tomography,'' *J. Biomed. Opt.* **1**, 157–173 (1996).
18. F. Fercher and C. K. Hitzenberger, ''Measurement and imaging of birefringence and optic axis orientation by phase resolved polarization sensitive optical coherence tomography,'' in *Proc. Intl. Trends in Optics and Photonics ICO IV*, T. Asakura, Ed., Springer, Berlin (1999).
19. J. F. de Boer, S. M. Srinivas, B. H. Park, T. H. Pham, Z. Chen, T. E. Milner, and J. S. Nelson, ''Polarization effects in optical coherence tomography of various biological tissues,'' *IEEE J. Sel. Top. Quantum Electron.* **5**, 1200–1203 (1999).
20. M. J. Everett, K. Schoenenberger, B. W. Colston, Jr., and L. B. Da Silva, ''Birefringence characterization of biological tissue by use of optical coherence tomography,'' *Opt. Lett.* **23**, 228–230 (1998).
21. K. Schoenenberger, B. W. Colston, Jr., D. J. Maitland, L. B. Da Silva, and M. J. Everett, ''Mapping of birefringence and thermal damage in tissue by use of polarization-sensitive optical coherence tomography,'' *Appl. Opt.* **37**, 6026–6036 (1998).
22. M. R. Hee, D. Huang, E. A. Swanson, and J. G. Fujimoto, ''Polarization-sensitive low-coherence reflectometer for birefringence characterization and ranging,'' *J. Opt. Soc. Am. B* **9**, 903–908 (1992).
23. A. G. Ushenko, ''Laser biospeckles fields vector structure and polarization diagnostics of skin collagen structure,'' *Laser Phys.* **10**(5), 1143–1149 (2000).
24. O. V. Angelsky, D. M. Burkovets, V. P. Pishak, Y. A. Ushenko, and O. V. Pishak, ''Polarization-correlation investigations of biotissue multifractal structures and their pathological changes diagnostics,'' *Laser Phys.* **10**(5), 1136–1142 (2000).
25. O. V. Angelsky, A. G. Ushenko, and D. M. Burkovets, ''Polarization-correlation analysis of anisotropic structures in bone tissue for the diagnostics of pathological changes,'' *Opt. Spektrosk.* **90**(3), 458–464 (2001).
26. S. Bartel and A. H. Hielscher, ''Monte Carlo simulations of the diffuse backscattering Mueller matrix for highly scattering media,'' *Appl. Opt.* **39**, 1580–1588 (2000).
27. G. Yao and L.-H. Wang, ''Propagation of polarized light in turbid media: simulated animation sequences,'' *Opt. Express* **7**, 198–203 (2000).
28. A. Ambirajan and D. C. Look, ''A backward Monte Carlo study of the multiple scattering of a polarized light beam,'' *J. Quantum Spectrosc. Radiat. Trans.* **58**, 171–192 (1997).
29. X. Wang, L.-H. Wang, C.-W. Sun, and C. C. Yang, ''Polarized light propagation through scattering media: time-resolved Monte Carlo simulations and experiments,'' *J. Biomed. Opt.* **8**(4), 608–617 (2003).
30. X. Wang, G. Yao, and L.-H. Wang, ''Monte Carlo model and single-scattering approximation of the propagation of polarized light in turbid media containing glucose,'' *Appl. Opt.* **41**(4), 792–801 (2002).
31. X. Wang and L.-H. Wang, ''Propagation of polarized light in birefringent turbid media: a Monte Carlo study,'' *J. Biomed. Opt.* **7**(3), 279–290 (2002).
32. G. Yao and L.-H. Wang, ''Two dimensional depth resolved Mueller matrix measurement in biological tissue with optical coherence tomography,''*Opt. Lett.* **24**, 537–539 (1999).
33. D. Cameron, M. J. Rakovic, M. Mehrubeoglu, G. Kattawar, S. Rastegar, L. V. Wang, and G. L. Cote, ''Measurement and calculation of the two-dimensional backscattering Mueller matrix of a turbid medium,'' *Opt. Lett.* **23**, 485–487 (1998).
34. J. F. de Boer, T. E. Milner, and J. S. Nelson, ''Determination of the depth-resolved Stokes parameters of light backscattered from turbid media by use of polarization-sensitive optical coherence tomography,'' *Opt. Lett.* **24**, 300–302 (1999).
35. S. Jiao, G. Yao, and L. V. Wang, ''Depth-resolved two-dimensional Stokes vectors of backscattered light and Mueller matrices of biological tissue measured with optical coherence tomography,'' *Appl. Opt.* **39**, 6318–6324 (2000).
36. S. Jiao and L.-H. Wang, ''Two-dimensional depth-resolved Mueller matrix of biological tissue measured with double-beam polarization-sensitive optical coherence tomography,'' *Opt. Lett.* **27**(2), 101–103 (2002).
37. S. Jiao, W. Yu, G. Stoica, and L.-H. Wang, ''Contrast mechanisms in polarization-sensitive Mueller-matrix optical coherence tomography and application in burn imaging,'' *Appl. Opt.* **42**(25), 5191–5197 (2003).
38. S. Jiao, W. Yu, G. Stoica, and L.-H. Wang, ''Optical-fiber-based Mueller optical coherence tomography,'' *Opt. Lett.* **28**(14), 1206–1208 (2003).
39. E. Okada, M. Firbank, M. Schweiger, et al. ''Theoretical and experimental investigation of near-infrared light propagation in a model of the adult head,'' *Appl. Opt.* **36**(1), 21–31 (1997).
40. A. Kienle and R. Hibst, ''New optical wavelength for treatment of portwine stains,'' *Phys. Med. Biol.* **40**, 1559–1576 (1995).
41. S. L. Jacques, C. A. Alter, and S. A. Prahl, ''Angular dependence of HeNe laser light scattering by human dermis,'' *Lasers Life Sci.* **1**, 309–333 (1987).
42. R. Marchesini, A. Bertoni, S. Andreola, et al. ''Extinction and absorption coefficients and scattering phase functions of human tissues *in vitro*,'' *Appl. Opt.* **28**, 2318–2324 (1989).